E3S Web of Conferences **675**, 03009 (2025) https://doi.org/10.1051/e3sconf/202567503009
GeoME'5.5 2025

AI-Driven Time-Variant Reliability Assessment of an Elevated Water Tank Over Its Service Life Using Radial Basis Function and Artificial Neural Networks

Najib ZEMED[1*], *Kaoutar* MOUZOUN[1], *Hanane* MOULAY ABDELALI[1], *Toufik* CHERRADI[1], *Azzeddine* BOUYAHYAOUI[1]

[1]Civil Engineering and Construction Laboratory (LGCC), Mohammadia School of Engineering, Mohammed V University, Rabat, Morocco

Abstract. This study introduces a time-dependent reliability assessment of elevated reinforced-concrete water towers, highlighting the combined influence of material behaviour and environmental actions. The proposed framework integrates Kriging and Artificial Neural Networks within an active-learning ensemble, enabling a substantial reduction in computational effort while preserving the accuracy of Monte Carlo simulations. The analysis is based on a concrete crack-width limit state and explicitly incorporates long-term material effects, including concrete creep, as well as realistic wind conditions whose variability is adjusted according to projected climate-change scenarios. Relative humidity is also considered to capture its influence on creep development and serviceability performance. Results show a marked reduction in reliability under low-humidity conditions due to increased deformation, and a significant contribution of climate-induced wind variability to structural demand. Sensitivity analyses indicate that geometric parameters, particularly tank height and radius, play a major role in failure probability, whereas improvements in material properties help to reduce crack widths and enhance durability. A maintenance strategy based on a target reliability index is finally examined, demonstrating its effectiveness in improving performance when re-evaluated over the service life.

1 Introduction

Elevated water tanks are long-lived components of urban water systems, operating continuously to buffer short-term variations in demand. Over years of service, the concrete is exposed to persistent actions that activate time-dependent material phenomena. Creep produces slow, irreversible deformations in the cementitious matrix, while drying shrinkage caused by moisture loss leads to additional volumetric changes. Acting together, these mechanisms modify the strain state of the material and promote micro-cracking, which can gradually evolve into visible cracks.

[*] Najib ZEMED: najibzem@gmail.com

Traditionally, reliability assessments relied on methods like FORM, SORM, and MCS. In short, FORM and SORM use Taylor expansions [1], FORM with a first-order (linear) approximation, SORM by adding second-order curvature for better accuracy. That said, both approaches tend to struggle when the limit state is highly nonlinear or when the dimension grows. By contrast, MCS (Level III method) remains robust and non-approximate [2], but it quickly becomes computationally prohibitive for time-dependent problems that demand many simulations.

To get around these limits, AI-based surrogate models (also called metamodels) have emerged [3]. They approximate the target function with far fewer simulations while keeping strong predictive precision. Common choices include SVR [4], RBFNs [5], Kriging [6], , and ANNs [7]. These models are particularly handy when the limit state is complex yet training data must stay minimal. Additionally, Kriging provides an uncertainty estimate that is useful for adaptive sampling.

Of course, even if surrogates cut the computational cost [8], they can lose precision near the failure surface. This is where active learning comes in: it refines the surrogate iteratively by sampling where uncertainty is high. Well-known frameworks include AK-MCS [6] and AK-SYS [9], both mixing surrogate modeling with targeted enrichment.

Recently, time-dependent reliability has gained traction, notably for reinforced concrete bridges. The point is to account for the progressive degradation of materials under long-term mechanical and environmental actions. Surprisingly, despite facing similar degradation phenomena, elevated water tanks have received much less attention. Most contributions still focus on bridges. For example, Fatima et al. [10] integrate realistic traffic loads plus creep, shrinkage, and corrosion to assess time-dependent reliability. Likewise, Liu et al. [11] discretize stochastic processes to capture WIM-based load variability and evaluate reliability over time. More recently, Zemed et al. [12] combined ensemble surrogate models to estimate the time-variant reliability of an RC bridge under multiple degradation mechanisms, and proposed a predictive-maintenance framework to mitigate failure risks. Taken together, these advances show the potential of time-dependent reliability. Yet, similar approaches remain underexplored for elevated water tanks even though they are exposed to the same long-term effects. Extending these analyses is essential to ensure durable and safe operation over the service life.

In contrast, most studies on elevated water tanks still rely on static analyses, with only a partial description of long-term material degradation. Often, probabilistic tools are applied, but the combined influence of creep, drying shrinkage and reinforcement corrosion on materials behaviour is simplified, and the effect of maintenance actions on future reliability is ignored. For example, Hammoum et al. [13] considered wind variability but not deterioration of the concrete–steel assembly, and Way and Viljoen [14] examined crack-width reliability under EN 1992-3 without representing progressive aging. Another gap is the lack of models that update reliability after maintenance, even though materials continue to evolve after each intervention and may regain performance.

In response to these gaps, the present work introduces a time-dependent reliability approach for elevated water tanks that focuses on material behaviour and durability. The method uses AI-based surrogate modelling to reproduce the response of reinforced-concrete materials. Radial Basis Function Networks and Artificial Neural Networks are combined in an active-learning strategy that refines the surrogate and predicts failure probabilities across the service life. The active-learning loop adds simulations at key points of the material–loading space, and the framework incorporates maintenance scenarios so that reliability can be re-evaluated after each repair or rehabilitation action.

2 Problem Definition and Modeling Framework

This study evaluates the reliability over time of an elevated reinforced concrete water tower using an active learning approach based on a set of AI metamodels.

2.1 Geometric and Numerical Modeling of the Water Tower

The water tower considered here comprises two main parts. First, a cylindrical reinforced concrete shaft provides vertical support and global stability. Second, an inverted truncated-cone tank maximizes storage volume while promoting a more uniform load distribution. The overall geometry is shown in Fig. 1.

To simulate the material response, we developed a numerical model in ANSYS APDL using SHELL181 elements, which are well suited for thin-walled concrete components. The shaft, tank, and dome were modeled together to preserve geometric continuity and capture the stress transfer between parts.

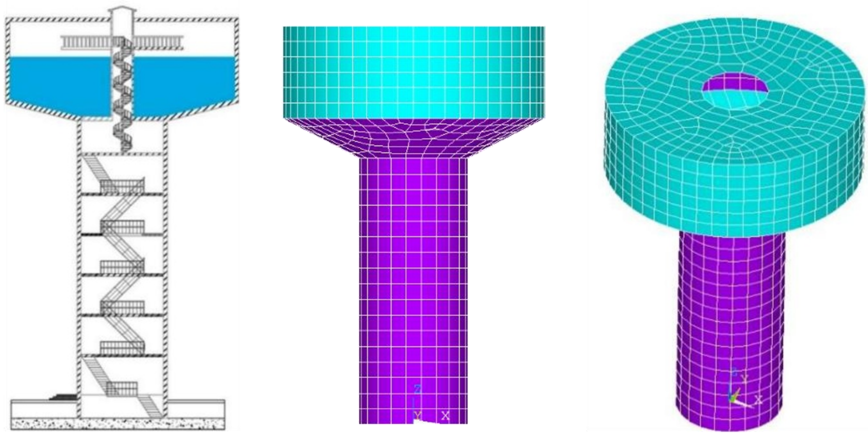

(a). Cross-sectional view (b). Finite element model in ANSYS APDL

Fig. 1. Geometric and numerical representation of the studied elevated water tank.

2.2 Loading and Degradation Models

The analysis of the water tower considers the following loads and degradation effects:

- **Self-weight**: A gravity load is applied using $g = 9.81\ m/s^2$.
- **Hydrostatic pressure**: Water pressure is applied on the inner surface of the storage tank.
- **Wind pressure**: Defined as per Eurocode 1, the wind pressure at height z and angle α is:

$$W_e(z,\alpha) = q_p(z)\, C_{pe}(\alpha) \tag{1}$$

where $C_{pe}(\alpha)$ is the external pressure coefficient and $q_p(z)$ is the peak velocity pressure at height z.

- **Creep effect:** Time-dependent creep is modeled using the CEB-FIP90 formulation:

$$\varphi(t,t_0) = \varphi_0\, \beta_c(t-t_0) \tag{2}$$

where t_0 refers to the concrete's age at the moment of load application, φ_0 is a notional creep coefficient, and β_c.

- **Shrinkage effect**: Also based on the same model, shrinkage strain is defined as:

$$\varepsilon_{cs}(t,t_s) = \varepsilon_{cs0}\, \beta_s(t-t_s) \tag{3}$$

where t_s refers to the time at which shrinkage begins, ε_{cs0} is the theoretical final shrinkage strain, and β_s represents a function that models how shrinkage evolves with time.

- **Steel corrosion:** Reinforcement degradation is modeled using Stewart's formulation, which describes the reduction of the steel diameter over time as:

 https://doi.org/10.1051/e3sconf/202567503009

$$D(t) = \begin{cases} D_i & ,if\ :\ t < T_i \\ D_i - 0.0232\ i_{corr}\ (t - T_i) & ,if\ :\ T_i < t < T_i + \dfrac{D_i}{0.0232} \\ 0 & ,if\ :\ t > T_i + \dfrac{D_i}{0.0232} \end{cases} \tag{4}$$

where D_i is the initial diameter, i_{corr} is the propagation speed of the corrosion phenomenon, and T_i is the time required for corrosion to begin.

2.3 Limit State Function

In this paper, we assume that failure occurs whenever the tensile demand on the tank structure outweighs the tensile strength of the surrounding reinforcement. As a result, the limit state function is written as:

$$G(X,t) = \frac{A_s(X,t)f_{yk}}{\gamma_s} - N_{max}(X,t) \tag{5}$$

where A_s is the cross-sectional area of circumferential reinforcement per linear meter, accounting for corrosion degradation, f_{yk} is the characteristic yield strength of the reinforcement steel, γ_s is the partial safety factor applied to reinforcement, N_{max} is the maximum internal tensile force per meter in the tank wall, extracted from the finite element model developed in ANSYS APDL.

3 Proposed Active Learning-Based Reliability Methodology

The present paper introduces an active learning approach based on an iterative and adaptive sampling strategy. The algorithm is illustrated in Fig. 2 and detailed below.

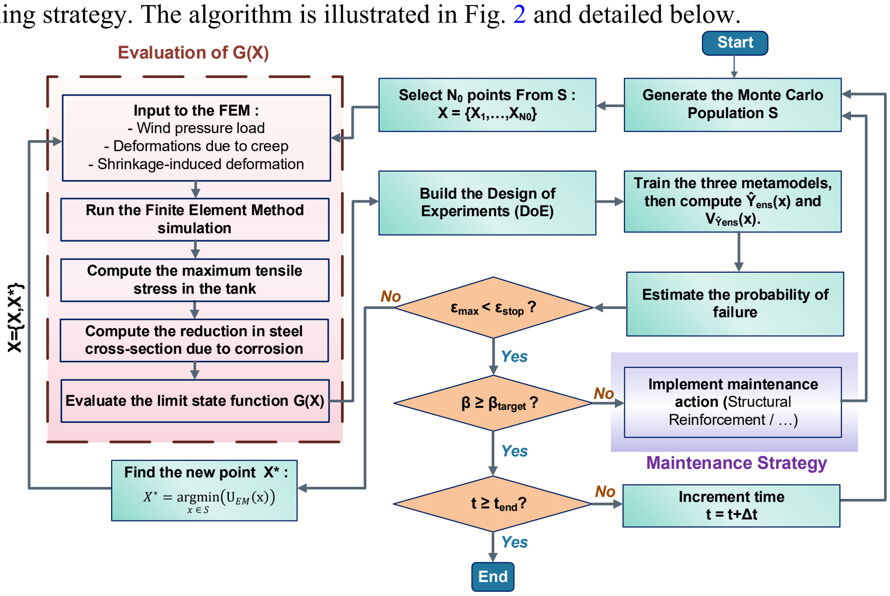

Fig. 2. Framework of the Proposed Active Learning-Based Reliability Assessment.

(1). **Generate the Monte Carlo population:** The initial sample population S, consisting of N points, is generated.

(2). **Selection of the Initial Training Set:** A small subset N_0 is then selected from the population S to serve as the starting design set. For example, $N_0 = 10$ samples can be chosen.

(3). **Evaluation of the limit state function:** Each selected sample is evaluated through a FEM developed in ANSYS APDL. The model incorporates key physical effects, including Wind loading, Time-dependent deformation due to creep, Strain induced by shrinkage. The model is used to extract the maximum tensile stress. In parallel, the corrosion-induced reduction in reinforcement cross-section is computed to determine the residual tensile resistance of the steel. These quantities are combined to evaluate the performance function G(X) at each sample point.

(4). **Construction of the Design of Experiments (DoE):** Once the limit state function has been evaluated for all initial points, the DoE is constructed $\{X, Y = G(X)\}$.

(5). **Construction of Artificial Intelligence Surrogate Models:** In this study, three different surrogate models are developed and combined into a single robust averaged surrogate. This strategy improves prediction accuracy and, most importantly, allows for the estimation of local prediction variance, which plays a central role in the active learning process, the steps are:

- **Training of the Metamodels:** Three metamodels are constructed: one Artificial Neural Network (ANN) and two Radial Basis Function Networks (RBF-NNs), their architecture is illustrated in Fig. 3. The ANN consists of an input layer, one to three hidden layers (with 15–25 neurons each), and an output layer. It uses the sigmoid activation function. Training is carried out using a grid search strategy combined with cross-validation, and the optimal configuration is selected by minimizing the RMSE using the Levenberg-Marquardt algorithm. The two RBF models share the same three-layer architecture but differ in their activation functions: one uses the Gaussian kernel, while the other employs the multiquadric function, the centers of these activation functions are determined using K-means clustering, and the weights are computed analytically via the least squares method, avoiding iterative optimization.
- **Building an Ensemble Surrogate Model:** The three models are combined using:

$$\hat{Y}_{ensemble}(x) = \sum_{j=1}^{M} w_j(x) \times \hat{y}_j(x)$$
$$V_{\hat{Y}_{ensemble}}(x) = \sum_{j=1}^{M} w_j(x)\left[\hat{y}_j(x) - \hat{Y}_{ensemble}(x)\right]^2 \tag{6}$$

where $\hat{Y}_{ens}$ is the global prediction, $V_{\hat{Y}_{ens}}$ is the global variance prediction, $\hat{y}_j$ is the prediction of the j^{th} model, M is the number of models, and w_j is the weight assigned to each model.

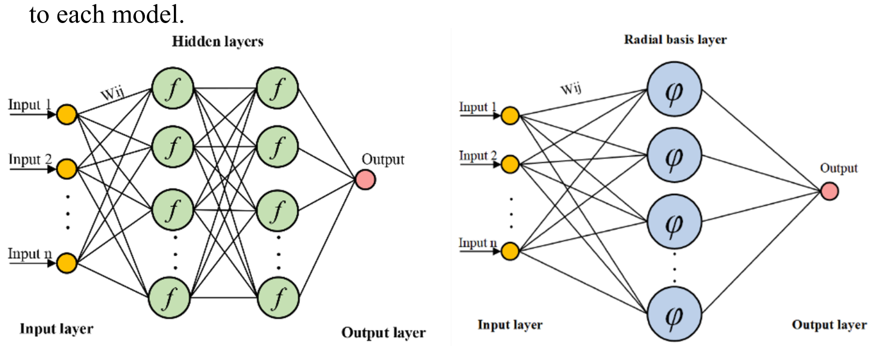

(a) Artificial Neural Networks. (b) Radial Basis Function Network

Fig. 3. Architecture of the artificial intelligence models used.

(6). **Failure Probability Computation:** At each step of the process, $\hat{P}_f$ is computed as:

$$\hat{P}_f = \sum_{i=1}^{N} \frac{I_{\hat{Y}_{ensemble}(x)\leq 0}(x_i)}{\mathrm{N}} \tag{7}$$

(7). **Stopping criterion:** The iterative process continues until the change in estimated failure probability over the last four iterations becomes sufficiently small. If this condition is satisfied, the algorithm proceeds. Otherwise, a new sampling point X^* is selected by minimizing the following function:

$$X^* = \underset{x \in S}{\operatorname{argmin}} \left[\frac{|\ \hat{Y}_{ensemble}(x)\ |}{\sqrt{V_{\hat{Y}_{ensemble}}(x)\ d_{min}(x)^2 \left(1 + \left\|\nabla^2\ \hat{Y}_{ensemble}(x)\right\|\right)}} \right] \tag{8}$$

where $d_{min}(x)$ refers to the minimum Euclidean distance between the point x and its closest neighbor in the DoE, and $\left\|\nabla^2\ \hat{Y}_{ensemble}(x)\right\|$ represents the norm of the Hessian matrix. And once the new point X^* is identified, return to step (3) to compute the limit state function.

(8). **Maintenance Strategy:** Once the failure probability is estimated, the reliability index is computed:

$$\beta = -\Phi^{-1}(\hat{P}_f) \tag{9}$$

If $\beta > \beta_{target}$ no action is needed. Otherwise, perform maintenance and return to Step (1) to reassess reliability.

4 Results

4.1 Definition of Random Variables for Reliability Analysis

In order to reflect the variability present in both material and environmental aspects of the water tower, this study considers fourteen distinct random variables. Each of these parameters - along with their associated statistics, measurement units, and bibliographic sources - is listed Table 1.

Table 1 Random variables distributions parameters of the water tower.

Variable	Description	Unit	Statistical Parameters	Distribution
E_{cm}	Young's modulus of concrete	MPa	$\mu = 30000\ \ \sigma = 1860$	Normal
E_s	Young's modulus of reinforcement	MPa	$\mu = 190000\ \sigma = 13680$	
e	Tank wall thickness	m	$\mu = 0.30\ \ \sigma = 0.015$	
R	Upper radius of the tank	m	$\mu = 8.5\ \ \sigma = 0.425$	
h	Tank height	m	$\mu = 10\ \ \sigma = 0.5$	
f_{cm}	Concrete's compressive resistance	MPa	$\mu = 30.5\ \ \sigma = 3.019$	
f_{yk}	steel's compressive resistance	MPa	$\mu = 550\ \ \sigma = 34.65$	
D_c	Cl- diffusion coefficient	cm²/yr	$\mu = 1.29\ \ CoV = 0.10$	Lognormal
D_i	Initial diameter of reinforcement bars	mm	$\mu = 2.772\ \ \sigma = 0.025$	
ρ_c	Concrete unit weight	kg/m³	$\mu = 2420.7\ \sigma = 42.1$	Normal
C	Concrete cover depth	mm	$\mu = 5\ \ \sigma = 0.65$	
C_0	Surface Cl- concentration	wt %	$\mu = 0.10\ \ CoV = 0.10$	Lognormal
C_{cr}	Critical Cl- concentration	wt %	$\mu = 0.40\ \ CoV = 0.10$	
$v_{mean,AMEE}$	Mean wind speed	m/s	$\lambda = 7.19\ k = 1.54$	Weibull

4.2 Time-Variant Reliability Assessment

Fig. 4 and Fig. 5 tell a consistent story. Over the first decades, the probability of failure grows only slightly while the reliability index β declines at a gentle pace. At the beginning, the slow change is expected for concrete in long-term service. Creep and shrinkage act in the background. Even as they approach their final asymptotic state, their impact on the limit-state check, based on exceeding the maximum internal stress, remains small. The reinforcement has not been significantly affected yet and continues to do its job, so the overall capacity is essentially preserved.

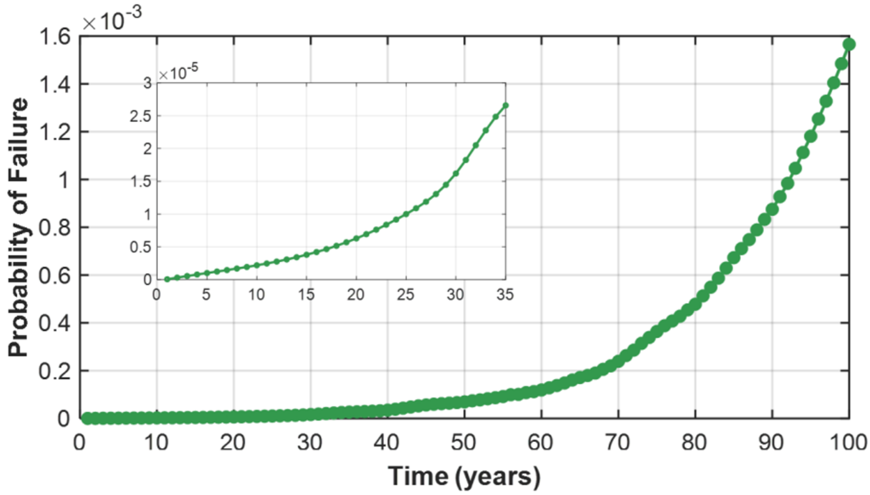

Fig. 4. Time-dependent evolution of failure probability for the Water Tower.

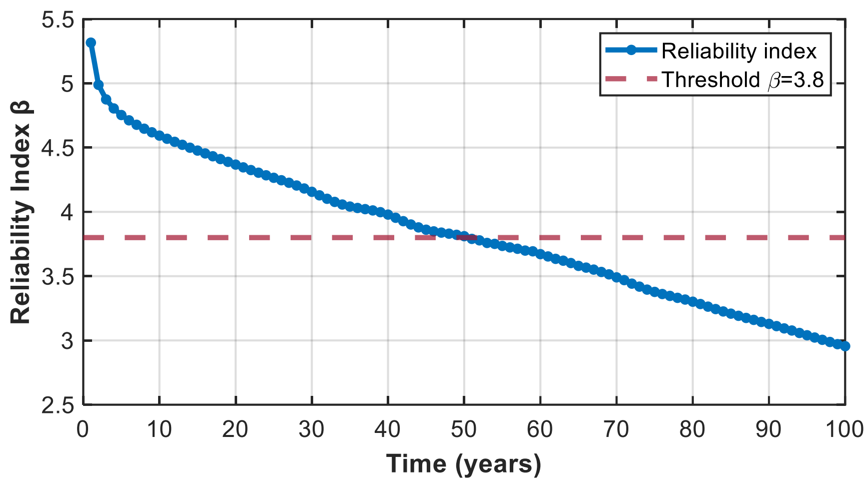

Fig. 5. Time-dependent evolution of the Reliability Index for the Water Tower.

A different regime begins around year 40. Corrosion initiates once chlorides reach the steel, from then on the bar diameter-and with it the tensile capacity-starts to fall. The consequence shows up clearly in the reliability curves: β drops faster, and the failure probability accelerates, especially beyond year 60.

If nothing is done, the trend continues. By year 100, our simulations give a failure probability of about 0.16%, and β falls below the reference threshold $\beta = 3.8$ (Eurocode 1,

 https://doi.org/10.1051/e3sconf/202567503009

EN 1990:2002). That crossing is a practical warning: inspection and maintenance should be planned before this point, not after.

Finally, the rate of deterioration is not purely due to the properties of the materials. Moisture, exposure to chlorides or other aggressive agents, and the tank's operating history can either mitigate or amplify these mechanisms. Since these factors vary from site to site, reliability updates must be calibrated to the specific environment rather than relying on a single generic curve.

4.3 Influence of Maintenance

Fig. 6 shows the effect of a maintenance action scheduled at year 50. Up to that point, the structure degrades under combined mechanical and environmental actions: long-term creep, shrinkage, and corrosion gradually erode its ability to meet service demands. To curb this trend, we adopt a two-step mid-life strategy. First, the maximum water level is capped at 70 % of full capacity, which immediately lowers hydrostatic pressure on the shell and thus the tensile demand. Second, we apply a surface chemical treatment to slow chloride ingress, reducing the concrete diffusion parameter D_c from μ = 1.29 cm²/year to μ = 0.8 cm²/year.

After the intervention, the picture is straightforward: the reliability index moves above the target, and the failure probability drops sharply and stays low for decades. In short, timely and relatively simple actions can meaningfully extend service life.

However, outcomes depend on timing and on how accurate the predictive model is. If deterioration is detected too late, or overestimated, costs may rise unnecessarily, if it's underestimated, service disruptions or failures become more likely.

Looking ahead, several options merit testing, for example FRP strengthening, electrochemical treatments, self-healing concretes, and mixes that replace part of the sand with recycled plastic waste, which have shown improvements in stiffness, crack resistance, and long-term behavior.

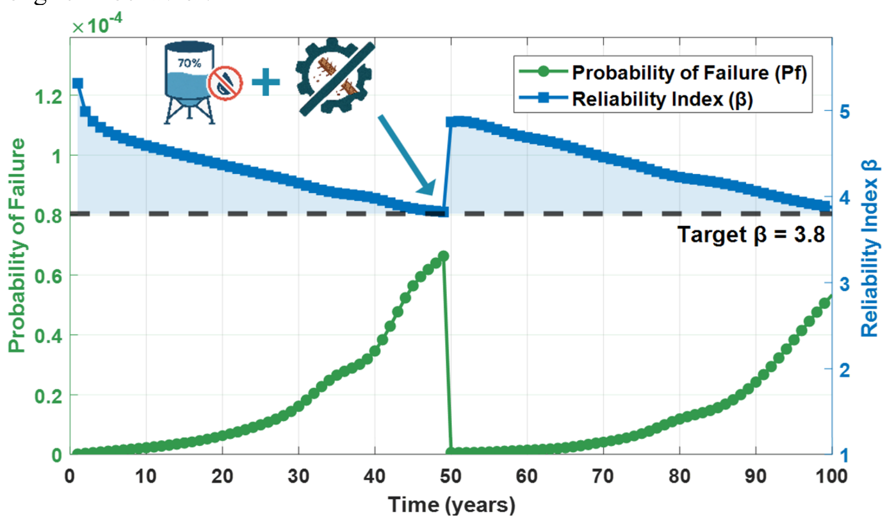

Fig. 6. Impact of Maintenance Intervention on Time-Dependent Failure Probability and Reliability Index.

5 Conclusions

This paper proposed a time-dependent reliability framework dedicated to reinforced-concrete water towers viewed as key components of gravity based and energy efficient water distribution systems. The approach combines advanced surrogate models, namely Radial Basis Function Networks and Artificial Neural Networks, with an active learning loop that concentrates simulations in the most informative zones and delivers accurate time-resolved estimates of failure probability with a significantly reduced computational effort. The formulation is built around the long term behaviour of cement based materials, including creep, shrinkage, cracking and reinforcement corrosion, and therefore connects naturally with a materials science perspective.

The numerical results reveal a clear and progressive degradation pattern in the reinforced-concrete materials over the service life. In the early years, modest mechanisms such as shrinkage and creep generate a slow decline in reliability. Once corrosion initiates, the load carrying capacity of the tank decreases more sharply, and if no action is taken the system eventually moves below commonly accepted reliability levels for water storage facilities that are essential for a secure and energy efficient supply of drinking water.

Under these conditions, the mid life maintenance scenario introduced at year 50 becomes a genuine turning point from both materials and energy viewpoints. Lowering the stored water level reduces the mechanical demand on the tank and at the same time limits the energy required for pumping, while the anti corrosion surface treatment slows down material degradation and delays the onset of critical cracking. Together, these measures produce a measurable recovery of the reliability index and extend the effective service life of the reinforced-concrete reservoir.

Beyond the specific case examined here, the study underlines the value of intelligent modelling tools for managing assets that combine complex material behaviour with long term energy and reliability constraints. By providing quantitative and time aware guidance on when to intervene, how to adapt operating conditions and which maintenance actions are most effective for materials rehabilitation, the proposed framework helps decision makers use maintenance budgets and energy resources more efficiently over the life cycle. Overall, the findings support a practical route toward safer and more sustainable management of elevated water tanks at the interface between energy use, materials durability and long term reliability.

References

1. R. Rackwitz; B. Flessler. Structural reliability under combined random load sequences. Computers & Structures. **9** (5). 489–94. (1978). https://doi.org/10.1016/0045-7949(78)90046-9
2. F. Lindsten; T. B. Schön. Backward Simulation Methods for Monte Carlo Statistical Inference. MAL. **6** (1). 1–143. (2013). https://doi.org/10.1561/2200000045
3. K. Mouzoun; A. Bouyahyaoui; H. Abdelali; T. Cherradi; K. Baba; I. Masrour; et al. How machine learning can transform the future of concrete. Asian Journal of Civil Engineering. **26**. 1395–411. (2025). https://doi.org/10.1007/s42107-025-01281-3
4. J.-M. Bourinet. Rare-event probability estimation with adaptive support vector regression surrogates. Reliab. Eng. Syst. Saf. **150**. 210–21. (2016). https://doi.org/10.1016/j.ress.2016.01.023
5. L. Cao; S. G. Gong; Y. R. Tao; S. Y. Duan. A RBFNN based active learning surrogate model for evaluating low failure probability in reliability analysis. Probabilistic Eng Mech. **74** (103496). (2023). https://doi.org/10.1016/j.probengmech.2023.103496
6. B. Echard; N. Gayton; M. Lemaire. AK-MCS: An active learning reliability method combining Kriging and Monte Carlo Simulation. Structural Safety. **33** (2). 145–54. (2011). https://doi.org/10.1016/j.strusafe.2011.01.002

7. J. B. Cardoso; J. R. de Almeida; J. M. Dias; P. G. Coelho. Structural reliability analysis using Monte Carlo simulation and neural networks. Advances in Engineering Software. **39** (6). 505–13. (2008). https://doi.org/10.1016/j.advengsoft.2007.03.015
8. B. Sudret; S. Marelli; J. Wiart. Surrogate models for uncertainty quantification: An overview. 2017 11th European Conference on Antennas and Propagation (EUCAP). 793–7. (2017). https://doi.org/10.23919/EuCAP.2017.7928679
9. W. Fauriat; N. Gayton. AK-SYS: An adaptation of the AK-MCS method for system reliability. Reliability Engineering & System Safety. **123**. 137–44. (2014). https://doi.org/10.1016/j.ress.2013.10.010
10. E. H. C. F; Y. R; M. H; H. C. F. Time-dependent reliability analysis for a set of RC T-beam bridges under realistic traffic considering creep and shrinkage. Eur J Environ Civ Eng. **26**. 6480–504. (2022). https://doi.org/10.1080/19648189.2021.1946720
11. F. Li; J. Liu; Y. Yan; J. Rong; J. Yi; G. Wen. A time-variant reliability analysis method for non-linear limit-state functions with the mixture of random and interval variables. Eng Struct. **213** (110588). (2020). https://doi.org/10.1016/j.engstruct.2020.110588
12. N. Zemed; H. M. Abdelali; T. Cherradi; A. Bouyahyaoui; K. Mouzoun. Time-Dependent Reliability and Sensitivity Analysis of Reinforced Concrete Bridges Considering Creep, Shrinkage, and Evolving Traffic Using Active Learning. Journal of Bridge Engineering. **31** (1). 04025093. (2026). https://doi.org/10.1061/JBENF2.BEENG-7698
13. H. Hammoum; K. Bouzelha; Y. Sellam; L. Haddad. Structural reliability of elevated water reservoirs under wind loading. Procedia Structural Integrity. **22**. 235–42. (2019). https://doi.org/10.1016/j.prostr.2020.01.030
14. A. C. Way; C. Viljoen. Reliability performance in tension governed reinforced concrete reservoirs as a function of target crack width. Structural Concrete. **24** (6). 7726–41. (2023). https://doi.org/10.1002/suco.202201159